

Interpolative approach for solving the Anderson impurity modelS. Y. Savrasov,¹ V. Oudovenko,^{2,5} K. Haule,^{3,5} D. Villani,^{4,5} and G. Kotliar⁵¹*Department of Physics, New Jersey Institute of Technology, Newark, New Jersey 07102, USA*²*Laboratory for Theoretical Physics, Joint Institute for Nuclear Research, 141980 Dubna, Russia*³*Jožef Stefan Institute, SI-1000 Ljubljana, Slovenia*⁴*JP Morgan Chase Bank, 270 Park Avenue, New York, New York 10017, USA*⁵*Department of Physics and Center for Material Theory, Rutgers University, Piscataway, New Jersey 08854, USA*

(Received 27 January 2004; revised manuscript received 20 December 2004; published 31 March 2005)

A rational representation for the self-energy is explored to interpolate the solution of the Anderson impurity model in the general orbitally degenerate case. Several constraints such as Friedel's sum rule and the positions of the Hubbard bands, as well as the value of the quasiparticle residue, are used to establish the equations for the coefficients of the interpolation. We employ two fast techniques, the slave-boson mean-field and the Hubbard I approximations, to determine the functional dependence of the coefficients on doping, degeneracy, and the strength of the interaction. The obtained spectral functions and self-energies are in good agreement with the results of the numerically exact quantum Monte Carlo method.

DOI: 10.1103/PhysRevB.71.115117

PACS number(s): 71.27.+a, 71.10.-w, 71.30.+h

I. INTRODUCTION

There has been recent progress in understanding the physics of strongly correlated electronic systems and their electronic structure near a localization-delocalization transition through the development of dynamical mean-field theory (DMFT).¹ Merging this computationally tractable many-body technique with electronic structure calculations of strongly correlated solids based on the local-density approximation² (LDA) is promising due to its simplicity and correctness in both band and atomic limits. At present, much effort is being made in this direction including the development of a LDA+DMFT method,³ the LDA++ approach,⁴ combined GW and DMFT theory,⁵ and spectral density functional theory,⁶ as well as applications to various systems such as La_{1-x}Sr_xTiO₃,⁷ V₂O₃,⁸ Fe and Ni,⁹ Ce,¹⁰ Pu,^{11,12} transition metal oxides,¹³ and many others. For a review, see Ref. 14.

Such *ab initio* DMFT-based self-consistent electronic structure algorithms should be able to explore the whole space of parameters where neither doping nor even the degeneracy itself is kept fixed, as different states may appear close to the Fermi level during iterations toward self-consistency. This is crucial if one would like to calculate properties of realistic solid state systems where the bandwidth and the strength of the interaction are not known at the beginning. It is very different from the ideology of model Hamiltonians where the input set of parameters defines the regime of correlations, and the corresponding many-body techniques may be applied afterward. Realistic DMFT simulations of material properties require fast scans of the entire parameter space to determine the interaction for a given doping, degeneracy, and bandwidth via the solution of the general multiorbital Anderson impurity model (AIM).¹⁵ Unfortunately, present approaches based on either the noncrossing approximation (NCA) or iterative perturbation theory (IPT) are unable to provide the solution to that problem due to the limited number of regimes where these methods can be applied.¹ The quantum Monte Carlo (QMC) technique^{1,16} is very accurate and can cope with multiorbital situations but

not with multiplet interactions. Also its applicability so far has been limited either to a small number of orbitals or to unphysically large temperatures due to its computational cost. Recently some progress has been achieved using impurity solvers that improve upon the NCA,¹⁷⁻¹⁹ but it has not been possible to retrieve Fermi liquid behavior at very low temperatures with these methods in the orbitally degenerate case.

As universal impurity solvers have not yet been designed we need to explore other possibilities, and this paper proposes an interpolative approach for the self-energy in the general multiorbital situation. We stress that this is not an attempt to develop an alternative method for solving the impurity problem, but a follow-up of the ideology of LDA theory where approximations were designed by analytical fits²⁰ to the quantum Monte Carlo simulations for a homogeneous electron gas.²¹ Numerically very expensive QMC calculations for the impurity model display smooth self-energies at imaginary frequencies for a wide range of interactions and dopings, and it is therefore tempting to design such an interpolation. We also keep in mind that for many applications a high precision in reproducing the self-energies may not be required. One such application is, for example, the calculation of the total energy,¹⁰⁻¹³ which, as is well known from LDA-based experience, may not be so sensitive to the details of the one-electron spectra. As a result, we expect that even crude evaluations of the self-energy shapes on the imaginary axis may be sufficient for solving many realistic total energy problems, some of which have appeared already.¹¹⁻¹³ Another point is the computational efficiency and numerical stability. Obtaining fully self-consistent loops with respect to charge densities¹¹ and other spectral functions requires many iterations toward convergence, which may not need very accurate frequency resolution at every step. However, the procedure that solves the impurity model should smoothly connect various regions of the parameter space. This is a crucial point if one would like to have a numerically stable algorithm and our interpolative approach ideally solves this problem.

In calculations of properties such as the low-energy spectroscopy and especially transport, a more delicate distribution of spectral weight takes place at low energies, and the imaginary part of the analytically continued self-energy needs to be computed with greater precision. Here we expect that our obtained spectral functions should be used with care. Also, in a few clearly distinct regimes, such as, e.g., very near the Mott transition, the behavior may be much more complicated and more difficult to interpolate. For the cases mentioned above, extensions of the interpolative method should be implemented, and this is beyond the scope of the present work.

We can achieve a fast interpolative algorithm for the self-energy by utilizing a rational representation. The coefficients in this interpolation can be found by forcing the self-energy to obey several limits and constraints. For example, if the infinite-frequency (Hartree-Fock) limit, the positions of the Hubbard bands, the low-frequency mass renormalization z , the mean number of particles \bar{n} , as well as the value of the self-energy at zero frequency $\Sigma(0)$ are known from independent calculation, the set of interpolating coefficients is well defined. In this work, we explore the slave-boson mean-field (SBMF) approach^{22–25} and the Hubbard I approximation²⁶ to determine the functional dependence of these coefficients upon doping, degeneracy, and the strength of the interaction U . We verify all trends produced by this interpolative procedure in the regimes of weak, intermediate, and strong interactions and at various doping conditions. These trends are compared with known analytical limits as well as against calculations using the quantum Monte Carlo method. Also compared with QMC results are the self-energies and spectral functions on both imaginary and real axes for selected values of the doping. The results indicate that the SBFM approach can predict such parameters of interpolation as \bar{n} , $\Sigma(0)$, and z with a good accuracy while the Hubbard I method fails in a number of regimes. However, the functional form of the atomic Green's function which appears within the Hubbard I approximation can be used to determine the positions of atomic satellites, which helps to impose additional constraints on our procedure.

Given the extraordinary computational speed of this approach we generally find a very satisfactory accuracy in comparisons with the numerically more accurate QMC calculations. If an increased accuracy is desired our method can be naturally extended by imposing more constraints and by implementing more refined impurity solvers other than the ones explored in this work.

The paper is organized as follows. In Sec. II we discuss rational interpolation for the self-energy and list the constraints. In Sec. III we discuss methods for solving the Anderson impurity model such as the slave-boson mean-field and Hubbard I approximations, which can be used to find these constraints. A brief survey of the QMC method used to benchmark our algorithm is also given. We present numerical comparisons of the SBFM and Hubbard I techniques against the QMC simulations for such quantities as the quasiparticle residue and multiple occupancies. In Sec. IV we report the results of the interpolative method and compare the obtained spectral functions with the QMC results. In Sec. V we discuss possible improvements of the algorithm. Section VI is the conclusion.

II. INTERPOLATIVE APPROACH

To be specific, we concentrate on the Anderson impurity Hamiltonian

$$H = \epsilon_f \sum_{\alpha=1}^N f_{\alpha}^{\dagger} f_{\alpha} + \frac{1}{2} U \sum_{\alpha \neq \beta} n_{\alpha}^f n_{\beta}^f + \sum_{\mathbf{k}\alpha} E_{\mathbf{k}\alpha} c_{\mathbf{k}\alpha}^{\dagger} c_{\mathbf{k}\alpha} + \sum_{\mathbf{k}\alpha} [V_{\alpha}^*(\mathbf{k}) f_{\alpha}^{\dagger} c_{\mathbf{k}\alpha} + V_{\alpha}(\mathbf{k}) c_{\mathbf{k}\alpha}^{\dagger} f_{\alpha}], \quad (1)$$

describing the interaction of the impurity level ϵ_f with bands of conduction electrons $E_{\mathbf{k}\alpha}$ via hybridization $V_{\alpha}(\mathbf{k})$. U is the Coulomb repulsion between different orbitals in the f band, and α is the orbital-spin index running from 1 to N . Inspired by the success of the iterative perturbation theory,¹ in order to solve the Anderson impurity model in the general multi-orbital case, we use a rational interpolative formula for the self-energy. This can be encoded into the form

$$\Sigma(\omega) = \frac{\sum_{m=0}^M a_m \omega^m}{\sum_{m=0}^M b_m \omega^m} = \Sigma(\infty) \frac{\prod_{m=1}^M [\omega - Z_m^{(\Sigma)}]}{\prod_{m=1}^M [\omega - P_m^{(\Sigma)}]}. \quad (2)$$

The coefficients a_m, b_m , or, alternatively, the poles $P_m^{(\Sigma)}$, zeros $Z_m^{(\Sigma)}$, and $\Sigma(\infty)$ in this equation are to be determined. The form (2) can be also viewed as a continued fraction expansion but this representation will not be necessary for the description of the method.

Our basic assumption is that only a clearly distinct set of poles in the rational representation (2) is necessary to reproduce the overall frequency dependence of the self-energy. Extensive experience gained from solving the Hubbard and periodic Anderson models within DMFT at various ratios of the on-site Coulomb interaction U to the bandwidth W shows the appearance of lower and upper Hubbard bands as well as a renormalized quasiparticle peak in the spectrum of one-electron excitations.¹

It is clear that the Hubbard bands are damped atomic excitations and to the lowest-order approximation appear as the positions of the poles of the atomic Green's function. In the $SU(N)$ symmetry case which is described by the Hamiltonian (1), these energies are denoted by the number of electrons occupying impurity level, i.e., $E_n = \epsilon_f n + \frac{1}{2} U n(n-1)$, and the atomic Green's function takes the simple functional form

$$G_{at}(\omega) = \sum_{n=0}^{N-1} \frac{C_n^{N-1} (X_n + X_{n+1})}{\omega + \mu - E_{n+1} + E_n}, \quad (3)$$

where X_n are the probabilities to find an atom in a configuration with n electrons while the combinatorial factor $C_n^{N-1} = (N-1)!/n!(N-n-1)!$ appears due to the equivalence of all states with n electrons in $SU(N)$.

We can represent the atomic Green's function (3) using the rational representation (2), i.e.,

$$G_{at}(\omega) = \frac{\prod_{n=1}^{N-1} [\omega - Z_n^{(G)}]}{N \prod_{n=1} [\omega - P_n^{(G)}]}, \quad (4)$$

where $P_n^{(G)}$ are all N atomic poles, while $Z_n^{(G)}$ denote $N-1$ zeros with N being the total degeneracy. The centers of the Hubbard bands are thus located at the atomic excitations $P_n^{(G)} = E_n - E_{n-1} - \mu = \epsilon_f - \mu - U(n-1)$. Using the standard expression for the atomic Green's function $G_{at}(\omega) = 1/[\omega + \mu - \epsilon_f - \Sigma_{at}(\omega)]$, we arrive at the desired representation for the atomic self-energy,

$$\Sigma^{(at)}(\omega) = \omega + \mu - \epsilon_f - \frac{\prod_{n=1}^N [\omega - P_n^{(G)}]}{N-1 \prod_{n=1} [\omega - Z_n^{(G)}]}. \quad (5)$$

Using this functional form for finite $\Delta(\omega)$ modifies the positions of poles and zeros via recalculating the probabilities X_n which is equivalent to the famous Hubbard I approximation (discussed in more detail in the next section).

We now concentrate on the description of the quasiparticle peak which is present in the metallic state of the system. For this an extra pole and zero have to be added in Eq. (5). To see this, let us consider the Hubbard model for the $SU(N)$ case where the local Green's function can be written by the Hilbert transform $G_f(\omega) = H[\omega + \mu - \epsilon_f - \Sigma(\omega)]$. If self-energy lifetime effects are ignored, the local spectral function becomes $N_f(\omega) = D[\omega + \mu - \epsilon_f - \text{Re } \Sigma(\omega)]$ where D is the noninteracting density of states. The peaks of the spectral functions thus appear as zeros in Eq. (5) and in order to add the quasiparticle peak, one needs to add one extra zero (denoted hereafter as X) to the numerator in Eq. (5). To make the self-energy finite at $\omega \rightarrow \infty$ one has to also add one more pole (denoted hereafter as $P_1^{(\Sigma)}$) which should appear in the denominator of Eq. (5). Furthermore, frequently the Hartree-Fock value for the self-energy can be computed separately and it is desirable to have a parameter in the functional form (5) which will allow us to fix $\Sigma(\infty)$. An obvious candidate to be changed is the self-energy pole in Eq. (5) that is closest to zero frequency. Let us denote this parameter by $P_2^{(\Sigma)}$ and rewrite the denominator of Eq. (5) as $(\omega - P_1^{(\Sigma)})(\omega - P_2^{(\Sigma)}) \prod_{n=1}^{N-2} [\omega - Z_n^{(G)}]$ where the product is now extended over all zeros of the atomic Green's functions except the one closest to zero, and two extra poles $P_1^{(\Sigma)}$ and $P_2^{(\Sigma)}$ can control the width of the quasiparticle peak and $\Sigma(\infty)$. Thus, we arrive at the functional form for the self-energy,

$$\Sigma(\omega) = \omega + \mu - \epsilon_f - \frac{(\omega - X) \prod_{n=1}^N [\omega - P_n^{(G)}]}{(P_1^{(\Sigma)} - \omega)(P_2^{(\Sigma)} - \omega) \prod_{n=1}^{N-2} [\omega - Z_n^{(G)}]}. \quad (6)$$

We are now ready to list all constraints of our interpolative scheme. To fix the unknown coefficients X , $P_1^{(\Sigma)}$, $P_2^{(\Sigma)}$, $P_n^{(G)}$, and $Z_n^{(G)}$ in Eq. (6) and to write down the linear set of equations for the coefficients a_m, b_m in Eq. (2) we use the following set of conditions.

(a) *Hartree-Fock value* $\Sigma(\infty)$. In the limit $\omega \rightarrow \infty$ the self-energy takes its Hartree-Fock form

$$\Sigma(\infty) = U(N-1)\langle n \rangle. \quad (7)$$

The mean level occupancy $\langle n \rangle$ is defined as the sum over all Matsubara frequencies for the Green's function, i.e.,

$$\langle n \rangle = T \sum_{i\omega} G_f(i\omega) e^{i\omega 0^+}, \quad (8)$$

where

$$G_f(\omega) = \frac{1}{\omega + \mu - \epsilon_f - \Delta(\omega) - \Sigma(\omega)} \quad (9)$$

defines the impurity Green function and $\Delta(\omega) = \sum_{\mathbf{k}} |V_{\alpha}(\mathbf{k})|^2 / (\omega - E_{\mathbf{k}\alpha})$ is the hybridization function [which is the same for all α within $SU(N)$].

(b) *Zero-frequency value* $\Sigma(0)$. The so-called Friedel sum rule establishes the relation between the total density and the real part of the self-energy at zero frequency,

$$\langle n \rangle = \frac{1}{2} + \frac{1}{\pi} \arctan \left(\frac{\epsilon_f + \text{Re } \Sigma(i0^+) + \text{Re } \Delta(i0^+)}{\text{Im } \Delta(i0^+)} \right) + \int_{-i\infty}^{+i\infty} \frac{dz}{2\pi i} G_f(z) \frac{\partial \Delta(z)}{\partial z} e^{z0^+}. \quad (10)$$

(c) *Quasiparticle mass renormalization value* $\partial \text{Re } \Sigma / \partial \omega|_{\omega=0}$. The slope of the self-energy at zero frequency controls the quasiparticle residue z using the following relationship:

$$\left. \frac{\partial \text{Re } \Sigma}{\partial \omega} \right|_{\omega=0} = 1 - z^{-1}. \quad (11)$$

Formally, constraints (b) and (c) hold for zero temperature only but we expect no significant deviations in many regions of parameters as long as we stay at low enough temperatures. The behavior may be more complicated in the vicinity of the Mott transition.²⁷

(d) *Positions of Hubbard bands*. As we discussed, in order that the self-energy obeys the atomic limit and places the centers of the Hubbard bands at the positions of the atomic excitations, we demand that

$$P_n^{(G)} + \mu - \epsilon_f = \Sigma(P_n^{(G)}). \quad (12)$$

This condition fixes almost all self-energy zeros $Z_m^{(\Sigma)}$ in Eq. (2) to the poles $P_n^{(G)}$. However, it alone does not ensure that the weight is correctly distributed among the Hubbard bands and that the very distant Hubbard bands disappear. For this to occur, distant poles of the Green's function have to be canceled out by nearby zeros of the Green's function. It is clear that each pole $P_n^{(G)}$ far from the Fermi level has to be accompanied by a nearby zero $Z_n^{(G)}$ in order for the weight of

the pole to be small. Thus, the self-energy has poles at the positions of Green's function zeros which can be encoded into the constraint

$$[\Sigma(Z_n^{(G)})]^{-1} = 0. \quad (13)$$

We want to keep this property of the self-energy for finite $\Delta(\omega)$ and thus demand that the self-energy diverges (when lifetime effects are kept, it only reaches a local maximum) at the zeros of the functional form (3) of $G_{at}(\omega)$. Note that the relationship (13) holds (approximately) for frequency ω larger than the renormalized bandwidth zW . Therefore the information about one $Z_n^{(G)}$ that lies close to $\omega=0$ is omitted and replaced by the information about $\Sigma(\infty)$, $\Sigma(0)$, and z as is done by separating $P_1^{(\Sigma)}$ and $P_2^{(\Sigma)}$ in the denominator of Eq. (6).

We can now write down a set of linear equations for all unknown coefficients in the expression (2). There is a total of $2M+2$ of parameters a_m and b_m , $m=0, M$, where we can always set $b_0=1$. The conditions (a), (b), and (c) give

$$a_0 = \Sigma(0), \quad (14)$$

$$b_0 = 1, \quad (15)$$

$$a_1 - \Sigma(0)b_1 = 1 - z^{-1}, \quad (16)$$

$$a_M - b_M \Sigma(\infty) = 0. \quad (17)$$

According to condition (d) we can use all N poles $P_n^{(G)}$ and $N-2$ zeros $Z_n^{(G)}$. The zero $Z_n^{(G)}$ closest to $\omega=0$ is dropped out. (There are small discontinuities that arise when the closest and next-closest zeros to the origin change their role. However, we found this effect to be very small, which will be evident from our plots presented in Sec. IV A.) This brings additionally $2N-2$ equations for the coefficients and makes $M=N$ as the degree of the rational interpolation, which is written below:

$$\sum_{m=0}^N a_m [P_n^{(G)}]^m - (P_n^{(G)} + \mu - \epsilon_f) \sum_{m=0}^N b_m [P_n^{(G)}]^m = 0$$

for $n = 1, \dots, N$, (18)

$$\sum_{m=0}^N b_m [Z_n^{(G)}]^m = 0 \quad \text{for } n = 1, \dots, N-2. \quad (19)$$

Note that while M may be rather large, the actual number of poles contributing to the self-energy behavior is indeed very small. We can directly see this from Eq. (5) which uses all N poles $P_n^{(G)}$ satisfying Eq. (12) and uses $N-2$ zeros $Z_n^{(G)}$ directly related to $N-2$ poles $P_m^{(\Sigma)}$. Clearly, when the spectral weight of the atomic excitation becomes small, the corresponding $P_n^{(G)}$ becomes close to $Z_n^{(G)}$ and cancellation occurs. Therefore in realistic situations when only the upper and lower Hubbard bands have significant spectral weight along with the quasiparticle peak, the actual degree of the polynomial expansion is either 2 or 3. However, it is advantageous numerically and cheap computationally to keep all poles and zeros in Eq. (6) because the formula automatically distributes

spectral weight over all existing Hubbard bands.

In the limit when $U \rightarrow 0$ the self-energy automatically translates to the noninteracting one. The atomic poles get close to each other but, most importantly, their spectral weight goes rapidly to zero as it gets accumulated within the quasiparticle band.

In the Mott insulating regime, the conditions (b) and (c) drop out while all poles $P_n^{(G)}$ and zeros $Z_n^{(G)}$ can be used to determine the interpolation. However, in this regime it does not matter whether one of $Z_n^{(G)}$ closest to $\omega=0$ is dropped out or kept, since we can always replace this information by information about $\Sigma(\infty)$. Therefore the Mott transition can be studied without changing the constraints.

We thus see that in the insulating case the self-energy correctly reproduces the well-known result of the Hubbard I method where the Green's function is computed after Eq. (9) with the atomic self-energy. If the lifetime effects are computed, the parameters $P_n^{(G)}$ and $Z_n^{(G)}$ become complex and the Hubbard bands will acquire an additional bandwidth. This effect is evident from the simulations using various perturbative or QMC impurity solvers and can be naturally incorporated into the interpolative formulas (2) or (6). However, in the practical implementation below we will omit it for illustrative purposes.

Let us now discuss the quality of interpolation from the perspective of the high-frequency behavior for the self-energy. The latter can be viewed³⁰ as an expansion in terms of the moments $\Sigma^{(m)}$, i.e.,

$$\Sigma(\omega \rightarrow \infty) = \sum_{m=0}^{\infty} \frac{\Sigma^{(m)}}{\omega^m}.$$

Most important for us is to look at the highest moments which are given by the Hartree-Fock value Eq. (7) involving the single-occupancy matrix $\langle n \rangle$, as well as the first moment

$$\Sigma^{(1)} = [(N-1)(N-2)\langle nn \rangle + (N-1)\langle n \rangle - (N-1)^2\langle n \rangle^2]U^2, \quad (20)$$

containing a double-occupancy matrix $\langle nn \rangle$. We see that the interpolation in part relies on the accuracy in computing multiple occupancies which are functionals of both the atomic excitations and the hybridization function. In this regard, using the exact atomic Green's function to find the poles $P_n^{(G)}$ and zeros $Z_n^{(G)}$ as part of the constrained procedure may not be as accurate since it would assume the use of *atomic* multiple occupancies which do *not* carry information about $\Delta(\omega)$. On the other hand, we can also use only a functional form of the atomic Green's function where the multiple occupancies are computed in a more rigorous manner. In the next section we will show how this can be implemented using the SBMF multiple occupancies which will be found to be in better agreement with the quantum Monte Carlo data.

Note that the moments $\Sigma^{(m)}$ themselves can be used in establishing the constraints for interpolation coefficients. This would involve independent evaluations of $\langle n \rangle$, $\langle nn \rangle$, $\langle nnn \rangle$, etc., as well as various integrals involving the hybridization function $\Delta(\omega)$. However, we may run into an ill-defined numerical problem since high-frequency infor-

mation will be used to extract the low-frequency behavior. Therefore, it is more advantageous numerically to use some poles and zeros of $G^{at}(\omega)$ as given by condition (d) above.

We thus see that the interpolational scheme is defined completely once a prescription for obtaining parameters such as $\Sigma(0)$, z , and $\langle n \rangle$ as well as the poles $P_n^{(G)}$ and zeros $Z_n^{(G)}$ is given. For this purpose we will test two commonly used methods: the SBMF method due to Gutzwiller²² as described by Kotliar and Ruckenstein²³ and the well-known Hubbard I approximation.²⁶ We compare these results against more accurate but computationally demanding quantum Monte Carlo calculations and establish the procedure to extract all necessary parameters.

Note that once the constraints such as z are computed from a given approximate method, some of the quantities such as the total number of particles $\langle n \rangle$ and the value of the self-energy at zero frequency, $\Sigma(0)$, can be computed fully self-consistently. They can be compared with their non-self-consistent values. If the approximate scheme already provides a good approximation for $\langle n \rangle$ and satisfies the Friedel sum rule, the self-consistency check can be avoided, hence accelerating the calculation. Indeed we found that inclusion of the self-consistency requirement improves the results only marginally except when we are in close vicinity to the Mott transition, but here we do not expect that our simple interpolative algorithm is very accurate.

We now give the description of the approximate methods for solving the impurity model and then present the comparisons of our interpolative procedure with the QMC calculations.

III. METHODS FOR SOLVING IMPURITY MODEL

A. Quantum Monte Carlo method

The quantum Monte Carlo method is a powerful and manifestly not perturbative approach in either the interaction U or the bandwidth W . In the QMC method one introduces a Hubbard-Stratonovich field and averages over it using Monte Carlo sampling. This is a controlled approximation using a different expansion parameter, the size of the mesh for the imaginary time discretization. Unfortunately it is computationally very expensive as the number of time slices and the number of Hubbard-Stratonovich fields increases. Also the method works only on the imaginary axis while analytical continuation is less accurate and has to be done with great care. An extensive description of this method can be found in Ref. 1. We will use this method to benchmark our calculations using approximate algorithms described later in this section. The parameter $\Delta\tau=0.25$ is used in all QMC simulations. For the calculations requiring a fixed mean number of electrons \bar{n} , the values of the chemical potential are adjusted to reach the desired number \bar{n} with an accuracy not worse than 0.3%.

B. Slave-boson mean field method

A fast approach to solve the general impurity problem is the slave-boson method.²³⁻²⁵ At the mean-field level, it gives results similar to the famous Gutzwiller approximation.²²

However, it is improvable by performing fluctuations around the saddle point. This approach is accurate as it has been shown recently to give the exact critical value of U in the large-degeneracy limit at half filling.²⁸

The main idea is to rewrite atomic states consisting of n electrons $|\gamma_1, \dots, \gamma_n\rangle$, $0 \leq n \leq N$, with the help of a set of slave bosons $\{\psi_n^{\gamma_1, \dots, \gamma_n}\}$. In the following, we assume the $SU(N)$ symmetric case, i.e., equivalence between different states $|\gamma_1, \dots, \gamma_n\rangle$ for fixed n . The formulas corresponding to the more general crystal-field case are given in the Appendix. The creation operator of the physical electron is expressed via slave particles in the standard manner.²⁴ In order to recover the correct noninteracting limit at the mean-field level, the Bose fields ψ_n can be considered as classical values found from minimizing a Lagrangian $L\{\psi_n\}$ corresponding to the Hamiltonian (1). Two Lagrange multipliers λ and Λ should be introduced in this way, which correspond to the following two constraints:

$$\sum_{n=0}^N C_n^N \psi_n^2 = 1, \quad (21)$$

$$\sum_{n=0}^N n C_n^N \psi_n^2 = TN \sum_{i\omega} G_g(i\omega) e^{i\omega 0^+} = \bar{n}. \quad (22)$$

The numbers ψ_n^2 are similar to the probabilities X_n discussed in connection with the formula for the atomic Green's function (3). We thus see the physical meaning of the first constraint, which is that the sum of probabilities of finding the atom in any state is equal to 1, and the second constraint gives the mean number of electrons coinciding with that found from $G_g(\omega) = [\omega - \lambda - b^2 \Delta(i\omega)]^{-1}$. The combinatorial factor $C_n^N = N! / n!(N-n)!$ comes due to the assumed equivalence of all states with n electrons.

Minimization of $L\{\psi_n\}$ with respect to ψ_n leads us to the following set of equations to determine the quantities ψ_n :

$$\begin{aligned} [E_n + \Lambda - n\lambda] \psi_n + nbT \sum_{i\omega} \Delta(i\omega) G_g(i\omega) [LR\psi_{n-1} + \psi_n bL^2] \\ + (N-n)bT \sum_{i\omega} \Delta(i\omega) G_g(i\omega) [R^2 b\psi_n + LR\psi_{n+1}] = 0, \end{aligned} \quad (23)$$

where $b = RL \sum_{n=1}^N C_{n-1}^{N-1} \psi_n \psi_{n-1}$ determines the mass renormalization, and the coefficients $L = (1 - \sum_{n=1}^N C_{n-1}^{N-1} \psi_n^2)^{-1/2}$, $R = (1 - \sum_{n=0}^N C_n^{N-1} \psi_n^2)^{-1/2}$ are normalization constants as in Refs. 23 and 24. $E_n = \epsilon_f n + Un(n-1)/2$ is the total energy of the atom with n electrons in the $SU(N)$ approximation.

Equation (23) along with the constraints (21),(22) constitute a set of nonlinear equations which have to be solved iteratively. In practice, we consider Eq. (23) as an eigenvalue problem with Λ being the eigenvalue and ψ_n being the eigenvectors of the matrix. The physical root corresponds to the lowest eigenvalue of Λ which gives a set of ψ_n determining the mass renormalization $Z=b^2$. Since the matrix to be diagonalized depends nonlinearly on ψ_n via the parameters L , R , and b and also on λ , the solution of the whole problem assumes self-consistency: (i) we build an initial approxima-

tion to ψ_n (for example the Hartree-Fock solution) and fix some λ ; (ii) we solve the eigenvalue problem and find new normalized ψ_n ; (iii) we mix the new ψ_n with the old ones using the Broyden method²⁹ and build new L , R , and b . Steps (ii) and (iii) are repeated until self-consistency with respect to ψ_n is reached. During the iterations we also vary λ to obey the constraints. The described procedure provides a stable computational algorithm for solving the AIM and gives us access to the low-frequency Green's function and the self-energy of the problem via knowledge of the slope of $\text{Im } \Sigma(i\omega)$ and the value $\text{Re } \Sigma(0)$ at zero frequency.

The described slave-boson method gives the following expression for the self-energy:

$$\Sigma(\omega) = (1 - b^{-2})\omega - \epsilon_f + \lambda b^{-2}. \quad (24)$$

The impurity Green's function $G_f(\omega)$ in this limit is given by the expression

$$G_f(\omega) = b^2 G_g(\omega). \quad (25)$$

As an illustration, we now give the solution of Eq. (23) for the nondegenerate case ($N=2$) and at the particle-hole symmetry point with $\epsilon_f - \mu = -(U/2)(N-1)$. Consider the dynamical mean-field theory for the Hubbard model which reduces the problem to solving the impurity model subject to the self-consistency condition with respect to $\Delta(\omega)$. Starting with the semicircular density of states (DOS), the self-consistency condition is given by Eq. (23). We obtain the following simplifications: $L=R=\sqrt{2}$, $\lambda=0$, $\psi_0=\psi_2$, $b=4\psi_1\psi_2$, and $G_g(\omega)=[\omega - (W/4)^2 b^2 G_g(\omega)]^{-1}$. The sum $T \sum_{i\omega} \Delta(i\omega) G_g(i\omega)$ appearing in Eq. (23) scales as $W\alpha/2$ with the constant α being the characteristic of a particular density of states and approximately equal to -0.2 in the semicircular DOS case. A self-consistent solution of Eq. (23) is therefore possible and simply gives $\psi_2^2 = U/32W\alpha + 1/4$. The Mott transition occurs when no sites with double occupancies can be found, i.e., when $\psi_0 = \psi_2 = 0$. The critical value of $U_c = 8W|\alpha|$. For $\alpha \approx -0.2$, this gives $U_c \approx 1.6W$ and reproduces the result for $U_{c2} = 1.49W$ known from the QMC calculation within a few percent accuracy. As the degeneracy increases, the critical U is shifted toward higher values.²⁸ From numerical calculations we obtained the following values of the critical interactions in the half-filled case: $U_c \approx 3W$ for $N=6$ (p level), $U_c \approx 4.5W$ for $N=10$ (d level), and $U_c \approx 6W$ for $N=14$ (f level).

The density-density correlation function $\langle nn \rangle$ for local states with n electrons is proportional to the number of pairs formed by n particles C_2^n / C_2^N . Since the probability for n electron orbitals to be occupied is given by $P_n = \psi_n^2 C_n^N$, the physical density-density correlator can be deduced from $\langle nn \rangle = \sum_n C_2^n / C_2^N P_n$. Similarly, the triple occupancy can be calculated from $\langle nnn \rangle = \sum_n C_3^n / C_3^N P_n$.

Let us now check the accuracy of this method by comparing its results with the QMC data. We consider the two-band Hubbard model in the $SU(N=4)$ orbitally degenerate case. The hybridization $\Delta(\omega)$ satisfies the DMFT self-consistency condition of the Hubbard model on a Bethe lattice

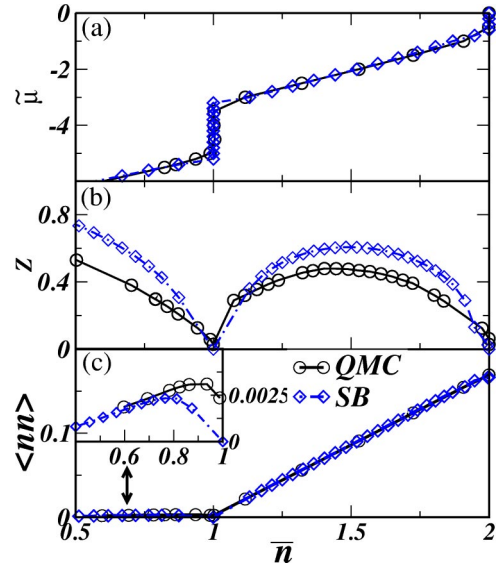


FIG. 1. (Color online) Comparison between the slave-boson mean-field and the QMC calculations for (a) concentration versus chemical potential $\bar{\mu} = \mu - \epsilon_f - (N-1)U/2$, (b) dependence of the spectral weight Z on concentration, and (c) density-density correlation function $\langle nn \rangle$ versus filling \bar{n} , in the two-band Hubbard model in $SU(4)$ and $U=4=2W$.

$$\Delta(\omega) = \left(\frac{W}{4}\right)^2 G(\omega). \quad (26)$$

The Coulomb interaction is chosen to be $U=2W$ which is sufficiently large to open the Mott gap at integer fillings. All calculations are done for the temperature $T=W/32$.

We first compare the average number of electrons vs chemical potential determined from the slave bosons, which is plotted in Fig. 1(a). This quantity is sensitive to the low-frequency part of the Green's function which should be described well by the present method. We see that it reproduces the QMC data with a very high accuracy and only differs by 20% very near the jump of $\bar{\mu}$ at $n=1$.

The quasiparticle residue z versus filling \bar{n} is plotted in Fig. 1(b). The slave-boson method gives a Fermi liquid and provides estimates for the quasiparticle residue with an overall discrepancy of the order of 30%. Here we would like to point out that (i) the extraction of zero-frequency self-energy slopes from the high-temperature QMC calculation is by itself numerically not a well-grounded procedure, as information for the self-energy is known at the Matsubara points only, which is then extrapolated to $\omega=0$; (ii) other methods for solving the impurity model, such as the NCA or IPT, display similar discrepancies; and (iii) recent findings²⁸ suggest that at least at half filling quasiparticle residues deduced from slave bosons become exact when $N \rightarrow \infty$. Most important for our interpolative method is that the entire functional dependence of z vs filling, interaction, and degeneracy is correctly captured. Its overall accuracy is acceptable as is evident from our comparisons of the spectral functions presented in the next section and well within the main goal of our work to provide fast scans of the entire parameter space necessary for simulating real materials.

Figure 1(c) shows the density-density correlation function $\langle nn \rangle$ as a function of average occupation \bar{n} . The discrepancy is most pronounced for fillings $\bar{n} \sim 1$ [see the inset of Fig. 1(c)] where the absolute values of $\langle nn \rangle$ are rather small. Although our slave-boson technique captures only the quasiparticle peak, it gives a correlation function in reasonable agreement with the QMC result for dopings not too close to the Mott transition.

C. Hubbard I approximation

Now we turn to the Hubbard I approximation²⁶ which is closely related to the moments expansion method.³⁰ Consider many-body atomic states $|\Phi_\kappa^{(n)}\rangle$ which in $SU(N)$ are all degenerate with index κ denoting these states for a given number of electrons n . The impurity Green's function is defined as the average

$$G_f(\tau) = -\langle T_\tau f_\alpha(\tau) f_\beta^\dagger(0) \rangle \quad (27)$$

and becomes diagonal with all equal elements in $SU(N)$. It is convenient to introduce the Hubbard operators

$$\hat{X}_{\kappa\kappa'}^{nn'} = |\Phi_\kappa^{(n)}\rangle\langle\Phi_{\kappa'}^{(n')}| \quad (28)$$

and represent the one-electron creation and destruction operators as follows:

$$f_\alpha = \sum_n \sum_{\kappa\kappa'} \langle\Phi_\kappa^{(n)}|f_\alpha|\Phi_{\kappa'}^{(n+1)}\rangle \hat{X}_{\kappa\kappa'}^{nn+1}, \quad (29)$$

$$f_\alpha^\dagger = \sum_n \sum_{\kappa\kappa'} \langle\Phi_\kappa^{(n+1)}|f_\alpha^\dagger|\Phi_{\kappa'}^{(n)}\rangle \hat{X}_{\kappa\kappa'}^{n+1n}. \quad (30)$$

The impurity Green's function (27) is given by

$$G_f(\tau) = \sum_{nm} G_{nm}(\tau), \quad (31)$$

where the matrix $G_{nm}(\tau)$ is defined as

$$G_{nm}(\tau) = - \sum_{\kappa_1\kappa_2\kappa_3\kappa_4} \langle\Phi_{\kappa_1}^{(n)}|f_\alpha|\Phi_{\kappa_2}^{(n+1)}\rangle \langle T_\tau \hat{X}_{\kappa_1\kappa_2}^{n+1n}(\tau) \hat{X}_{\kappa_3\kappa_4}^{m+1m}(0) \rangle \times \langle\Phi_{\kappa_3}^{(m+1)}|f_\alpha^\dagger|\Phi_{\kappa_4}^{(m)}\rangle. \quad (32)$$

Establishing the equations for $G_{nm}(\tau)$ can be performed using the method of equations of motion for the X operators. Performing their decoupling due to Hubbard,^{26,31} carrying out the Fourier transformation and analytical continuation to the real frequency axis, and summing over n and m after Eq. (31), we arrive at the net result

$$G_f^{-1}(\omega) = G_{at}^{-1}(\omega) - \Delta(\omega). \quad (33)$$

The $G_{at}(\omega)$ can be viewed in the matrix form (31) with the following definition of the diagonal atomic Green's function:

$$G_{nm}^{at}(\omega) = \delta_{nm} \frac{C_n^{N-1}(X_n + X_{n+1})}{\omega + \mu - E_{n+1} + E_n} \quad (34)$$

with $E_n = \epsilon_f n + U n(n-1)/2$ being the total energies of the atom with n electrons in $SU(N)$. The coefficients X_n are the

probabilities of finding an atom with n electrons and were already discussed in connection with the formula (3) for the atomic Green's function. They are similar to the coefficients ψ_n^2 introduced within the SBMF method but now found from a different set of equations. These numbers are normalized to unity, $\sum_{n=0}^N C_n^N X_n = \sum_{n=0}^{N-1} C_n^{N-1} (X_n + X_{n+1}) = 1$, and are expressed via the diagonal elements of $G_{nm}(i\omega)$ as follows:

$$X_n = -T \sum_{i\omega} G_{nn}(i\omega) e^{-i\omega 0^+} / C_n^{N-1}. \quad (35)$$

Their determination in principle assumes solving a nonlinear set of equations while determining $G_f(\omega)$. The mean number of electrons can be measured as $\bar{n} = \sum_{n=0}^N n C_n^N X_n$ or as $\bar{n} = TN \sum_{i\omega} G_f(i\omega) e^{i\omega 0^+}$. The numbers X_n can also be used to find the averages $\langle nn \rangle$, $\langle nnn \rangle$ in a way similar to what has been done in the SBMF approach.

If we neglect the hybridization $\Delta(\omega)$ in Eq. (33), the probabilities X_n become simply statistical weights:

$$X_n = \frac{e^{-(E_n - \mu n)/T}}{N \sum_{m=0}^N C_m^N e^{-(E_m - \mu m)/T}}. \quad (36)$$

We thus see that in principle there are several different ways to determine the coefficients X_n , either via self-consistent determination (35), or using the statistical formula (36), or taking them from the SBMF equation (23), i.e., setting $X_n = \psi_n^2$ while still utilizing the functional dependence provided by the Hubbard I method. To determine the best procedure let us first consider the limits of large and small U 's. When $\Delta(\omega) \equiv 0$, $G_f(\omega)$ is reduced to $\sum_{nm} G_{nm}^{at}(\omega)$, i.e., the Hubbard I method reproduces the atomic limit. Setting $U \equiv 0$ gives $G_f(\omega) = [\omega + \mu - \epsilon_f - \Delta(\omega)]^{-1}$, which is the correct band limit. Unfortunately, at half filling this limit has a pathology connected to the instability toward the Mott transition at any interaction strength U . To see this, we consider the dynamical mean-field theory for the Hubbard model. Using a semi-circular density of states, we obtain $G_f(\omega) = [1 - (W/4)^2 G_f(\omega) G_{at}(\omega)]^{-1} G_{at}(\omega)$ and conclude that for any small U the system opens a pathological gap in the spectrum. Clearly, using the Hubbard I method only, the behavior of the Green's function at $\omega \rightarrow 0$ cannot be reproduced and the quality of the numbers X_n is in question. This already emphasizes the importance of using the slave-boson treatment at small frequencies.

Ultimately, making the comparisons with the QMC calculations is the best option in picking the most accurate procedure to compute the probabilities X_n . To check the accuracy against the QMC result we again consider the two-band Hubbard model in $SU(4)$ symmetry as above. The chemical potential, mass renormalization, and double occupancy are plotted versus filling in Fig. 2. All quantities here were computed with the self-consistent determination of X_n after Eq. (35). We first see that the Hubbard I approximation does not give satisfactory agreement with the QMC data for $\bar{n}(\bar{\mu})$ because it misses the correct behavior at low frequencies.

The comparisons for $z(\bar{n})$ plotted in Fig. 2(b) surprisingly show a relatively good behavior. However, since the Hub-

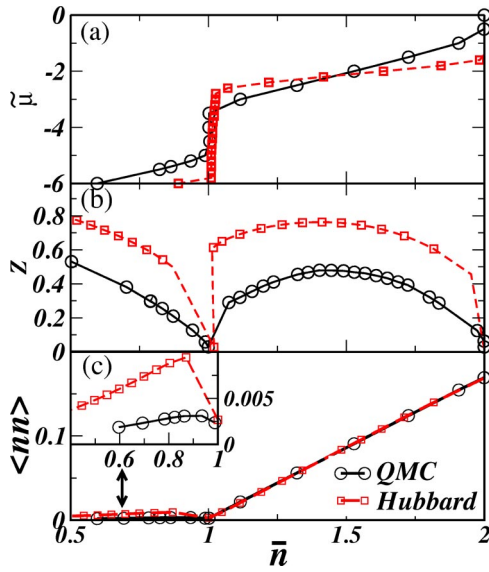


FIG. 2. (Color online) Comparison between the Hubbard I and the QMC calculations for (a) concentration versus chemical potential $\tilde{\mu} = \mu - \epsilon_f - (N-1)U/2$, (b) dependence of the spectral weight Z on concentration, and (c) density-density correlation function $\langle n_\alpha n_{\alpha'} \rangle$ versus filling \bar{n} , in the two-band Hubbard model in $SU(4)$ and for $U=2W=4$.

bard I approximation is never a Fermi liquid, it is not fair to talk about z in our context because there are no quasiparticles there. Figure 2(c) shows $\langle nn \rangle$ as a function of average occupation \bar{n} . As this quantity is directly related to the high-frequency expansion one may expect a better accuracy here. However, comparing Fig. 2(c) and Fig. 1(c), it is clear that the slave-boson method gives more accurate double occupancy. This is due to the fact that the density matrix obtained by the slave-boson method is of higher quality than the one obtained from the Hubbard I approximation.

The results of these comparisons suggest that the probabilities ψ_n^2 provided by the slave-boson method are a better way of determining the coefficients X_n in the metallic region of parameters. Therefore it is preferable to use these numbers while establishing the equations for the unknown coefficients in the interpolational form (2). However, the functional form (34) of the Hubbard I approximation with $X_n = \psi_n^2$ can still be used as it provides the positions of the poles $P_n^{(G)}$ and zeros $Z_n^{(G)}$ of the atomic Green's function necessary for the condition (d) in the previous section. This also ensures accurate high-frequency behavior of the interpolated self-energy since its moments expressed via multiple occupancies are directly related to ψ_n^2 .

Interestingly, while the more sophisticated QMC approach captures both the quasiparticle peak and the Hubbard bands this is not the case for the slave-boson mean-field method. To obtain the Hubbard bands in this method fluctuations need to be computed, which would be very tedious in the general multiorbital situation. However the slave-boson method delivers many parameters in good agreement with the QMC results, and, hence, it can be used to give the functional dependence of the coefficients of the rational approximation.

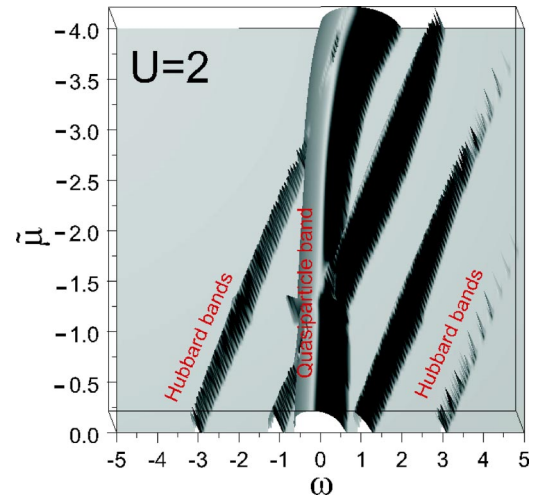


FIG. 3. (Color online) Calculated density of states using the interpolative method as a function of chemical potential $\tilde{\mu} = \mu - \epsilon_f - (N-1)U/2$ and frequency for the two-band Hubbard model in $SU(4)$ and at $U=W=2$.

IV. RESULTS OF THE INTERPOLATIVE SCHEME

By now the procedure to determine the coefficients is well established. We use the SBMF method to determine \bar{n} , $\Sigma(\infty)$, $\Sigma(0)$, and z as well as the poles and zeros of the atomic Green's function provided by the SBMF probabilities ψ_n^2 and by the bare atomic energy levels E_n (we omit the lifetime effects for simplicity). This generates a set of linear equations for coefficients a_m^α , b_m^α in the rational interpolation formula (2). In the present section we show the trends our interpolative algorithm gives for the spectral functions in various regions of parameters as well as provide detailed comparisons for some values of doping for both the imaginary and real axis spectral functions. The two-band Hubbard model with semicircular density of states and DMFT self-consistency condition after (26) is utilized in $SU(N=4)$ symmetry in all cases using the bandwidth $W=2$ and temperature $T=1/16$.

A. Trends

Figure 3 shows the behavior of the density of states $N(\omega) = -\text{Im} G_f(\omega) / \pi$ for $U=W$ as a function of the chemical potential $\tilde{\mu}$ computed with respect to the particle-hole symmetry point $(N-1)U/2$ and as a function of frequency ω . The semicircular quasiparticle band is seen at the central part of the figure. Its bandwidth is only weakly renormalized by the interactions in this regime. It is half filled for $\tilde{\mu}=0$ [i.e., when $\mu = \epsilon_f - (N-1)U/2$] and gets fully emptied when the chemical potential is shifted to negative values. Several weak satellites can also be seen on this figure, which are due to atomic poles. Their spectral weight is extremely small in this case and any sizable lifetime effect (which was not included while plotting this figure) will smear these satellites out almost completely. When approaching the fully emptied (or fully filled) situation the spectral weight of the Hubbard bands disappears completely and only the unrenormalized quasiparticle band remains. It is clear that even without shift-

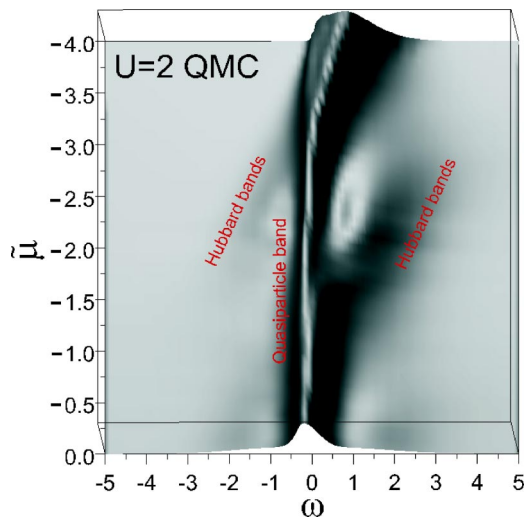


FIG. 4. (Color online) Calculated density of states using the QMC method as a function of chemical potential $\tilde{\mu} = \mu - \epsilon_f - (N-1)U/2$ and frequency for the two-band Hubbard model in SU(4) and at $U=W=2$.

ing the atomic poles to the complex axis, the numerical procedure of generating the self-energy is absolutely stable.

This trend can be directly compared with the simulations using a more accurate QMC impurity solver. We present this in Fig. 4 for $U=W$, which shows the calculated density of states in the same region of parameters. Remarkably, again we can distinguish the renormalized quasiparticle band and very weak Hubbard satellites. The Hubbard bands appear to be much more diffuse in this figure mainly due to the lifetime effects and partially due to the maximum entropy method used for analytical continuation from the imaginary to the real axis. Otherwise the entire picture looks very much like the one on Fig. 3, generated with much less computational effort.

Figure 5 gives the same behavior of the density of states for the strongly correlated regime $U=2W$. In this case the situation at integer filling is totally different as the system undergoes the metal-insulator transition. This is seen around the dopings levels with $\tilde{\mu}$ between 0 and -1 and between -3 and -5 where the width of the quasiparticle band collapses while lower and upper Hubbard bands acquire all the spectral weight. In the remaining region of parameters both the strongly renormalized quasiparticle band and Hubbard satellites remain. Again, once full filling or full emptying is approached the quasiparticle band has its original bandwidth restored while the Hubbard bands disappear. The QMC result for the same region of parameters is given in Fig. 6. Again we can distinguish the renormalized quasiparticle band and Hubbard satellites as well as the areas of Mott insulator and of strongly correlated metal. The Hubbard bands appear to be sharper in this figure, which signals the approach to the atomic limit.

B. Comparison for spectral functions on imaginary axis

We now turn to the comparison of the Green's functions and the self-energies obtained using the formulas (9) and (2),

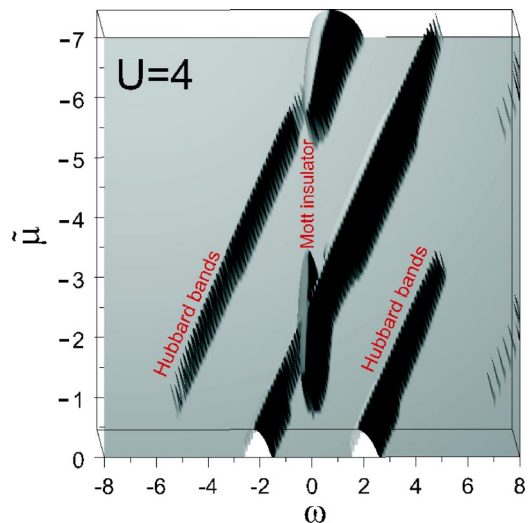


FIG. 5. (Color online) Calculated density of states using the interpolative method as a function of chemical potential $\tilde{\mu} = \mu - \epsilon_f - (N-1)U/2$ and frequency for the two-band Hubbard model in SU(4) and at $U=2W=4$.

respectively, against the predictions of the quantum Monte Carlo method. We will report our comparisons for the two-band Hubbard model and sets of dopings corresponding to $\bar{n}=0.5, 0.8, 0.95, 1.2, 1.5, 1.8$ using the value of $U=2W=4$. Other tests for different degeneracies, doping levels, and interactions have been performed and display similar accuracy.

Figure 7 shows the comparison between the real and imaginary parts of the Green's function obtained by the interpolative method with the results of the QMC calculations. As one can see, almost complete agreement has been obtained for a wide regime of dopings. The agreement gets less accurate once half filling is approached, but is still very good given the extraordinary computational speed of the interpolative method compared to QMC simulations.

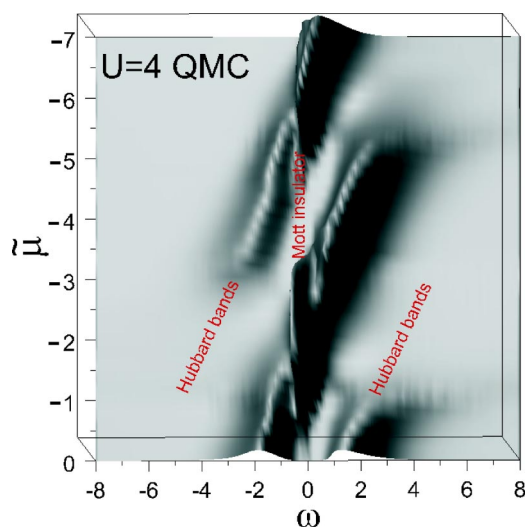


FIG. 6. (Color online) Calculated density of states using the QMC method as a function of chemical potential $\tilde{\mu} = \mu - \epsilon_f - (N-1)U/2$ and frequency for the two-band Hubbard model in SU(4) and at $U=2W=4$.

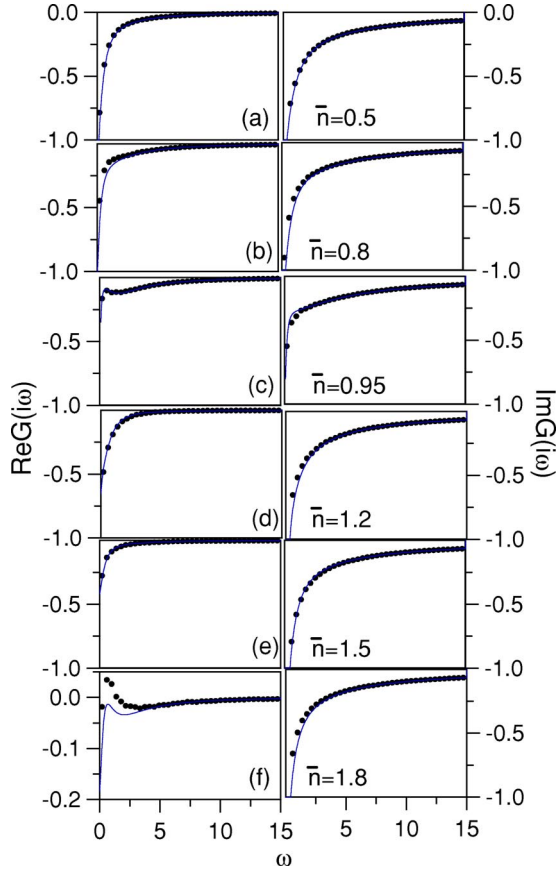


FIG. 7. (Color online) Comparison between real and imaginary parts of the Green's function obtained from the interpolative method and the quantum Monte Carlo calculation for the two-band Hubbard model at a set of fillings $\bar{n}=0.5, 0.8, 0.95, 1.2, 1.5, 1.8$ and $U=2W=4$.

Figure 8 shows similar comparison between the real and imaginary parts of the self-energies obtained by the interpolative and the QMC methods. We can see that the self-energies exhibit some noise which is intrinsic to the stochastic QMC procedure. The values of the self-energies near $i\omega = 0$ and ∞ are correctly captured with some residual discrepancies, attributed to slightly different chemical potentials used to reproduce the given filling within each method. The results on the imaginary axis show slightly underestimated slopes of the self-energies within the interpolative algorithm, which is attributed to the underestimated values of z obtained from the SBMF calculation. Ultimately, improving these numbers by inclusions of fluctuations beyond the mean field will further improve the comparisons. However, even at the present stage of accuracy, all the functional dependence given by the SBMF method quantitatively captures the behavior of the self-energy seen from the time-consuming QMC simulation.

C. Comparison for spectral functions on real axis

We also made detailed comparisons between the calculated densities of states obtained on the real axis using the interpolative method and the QMC algorithm. The QMC

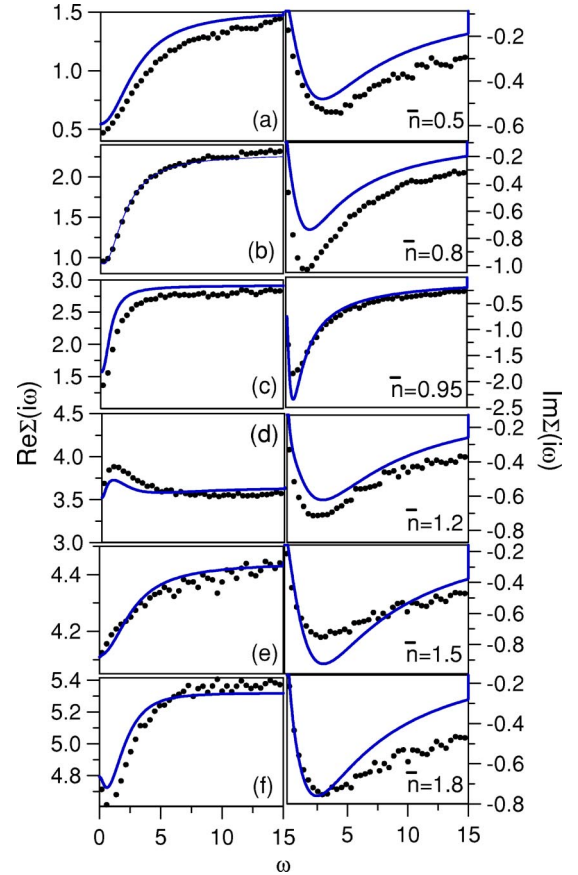


FIG. 8. (Color online) Comparison between real and imaginary parts of the self-energies obtained from the interpolative method and the quantum Monte Carlo calculation for the two-band Hubbard model at a set of fillings $\bar{n}=0.5, 0.8, 0.95, 1.2, 1.5, 1.8$ and $U=2W=4$.

densities of states require an analytical continuation from the imaginary to the real axis and were generated using the maximum entropy method. By itself this procedure introduces some errors within the QMC calculation especially at higher frequencies. In Fig. 9, we show our results for the fillings corresponding to $\bar{n}=0.5, 0.8, 0.95, 1.2, 1.5, 1.8$ using the value of $U=2W=4$. One can see the appearance of the quasiparticle band and two Hubbard bands distanced by the value of U . It can be seen that the interpolative method remarkably reproduces the trend in shifting of the Hubbard bands upon changing the doping. It automatically holds the distance between them to the value of U , while this is not always true in the quantum Monte Carlo method. Despite this result, the overall agreement between both methods is very satisfactory.

V. DISCUSSION

Here we would like to discuss possible ways to further improve the accuracy of the method. The inaccuracies are mainly seen in three different quantities: (i) the width of the Hubbard bands, (ii) the mass renormalization $z(\mu)$ which is borrowed from the SBMF method, and (iii) the number of electrons $n(\mu)$ extracted from the interpolated impurity

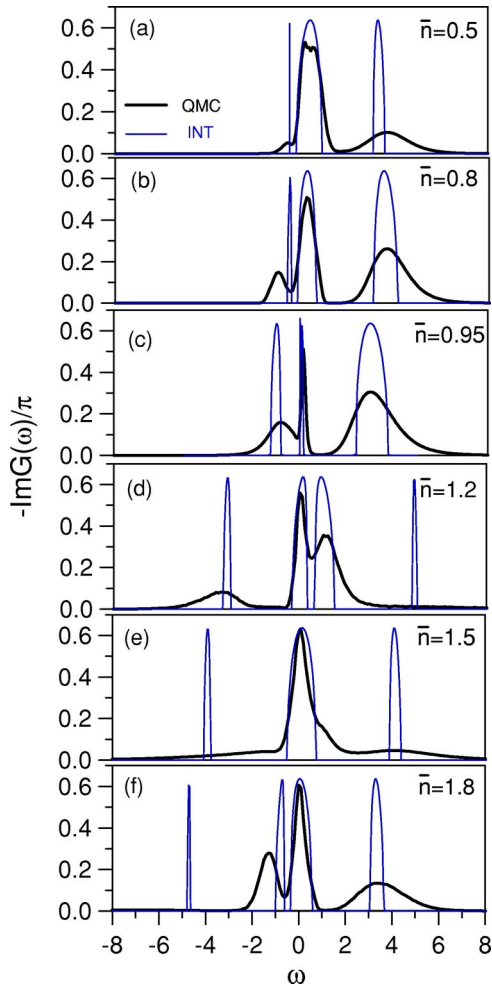


FIG. 9. (Color online) Comparison between the one-electron densities of states obtained from the interpolative formula and the quantum Monte Carlo calculation for the two-band Hubbard model at fillings $\bar{n}=0.5, 0.8, 0.95, 1.2, 1.5, 1.8$ and $U=2W=4$.

Green's function (9). The inaccuracy in the width of the Hubbard band is mainly connected to neglecting the lifetime effect. Provided it is computed, this will shift the positions of atomic poles onto the complex plane, which is in principle trivial to account for within our interpolative algorithm. To improve the accuracy of $z(\mu)$ one can, for example, work out a modified slave-boson scheme which will account for the fluctuations around the mean-field solution. The inaccuracy in $n(\mu)$ is small in many regions of parameters and typically amounts to 5-10%. We can try to improve this agreement by the requirement that $n(\mu)$ obtained via interpolation matches with $n_{SBMF}(\mu)$ obtained by the SBMF method. The latter agrees very well with the QMC result for a wide region of parameters as is evident from Fig. 1(a). In reality, our analysis shows that in many cases the discrepancy in $n(\mu)$ is connected with the overestimation of $z_{SBMF}(\mu)$. Therefore, points (ii) and (iii) mentioned above are interrelated.

The requirement that $n(\mu)=n_{SBMF}(\mu)$ can be enforced by adjusting the width of the quasiparticle band, and in many regions of parameters this is controlled by $z(\mu)$. However, there are situations when the Hubbard band appears in the

vicinity of $\omega=0$, and changing $z(\mu)$ does not affect the bandwidth. To gain control in those cases it is better to replace the constraints $\Sigma(0)$, $d\Sigma/d\omega|_{\omega=0}$ by the constraints of fixing the self-energies at two frequencies, say $\Sigma(0)$ and $\Sigma(i\omega_0)$, where ω_0 is a frequency of order of the renormalized bandwidth. We have found that this scheme gives mass renormalizations which are about 30% smaller than the SBMF ones, and the agreement with the QMC result is significantly improved. Thus, inaccuracies (ii) and (iii) can be avoided with this very cheap trick. However, we also would like to point out that the condition $n(\mu)=n_{SBMF}(\mu)$ is essentially nonlinear as the solution may not exist for all regions of parameters. It is, for example, evident that at such points where $n(\mu)$ is given by a symmetry (such as, e.g., the particle-hole symmetry point $n=2$ in the case considered above) the mass renormalization does not affect the number of electrons.

As the philosophy of our approach is to get the best possible fit we are also open to implementing any kinds of *ad hoc* renormalization constants. One such possibility could be the use of a quasiparticle residue 30% smaller than $z_{SBMF}(\mu)$. As $z(\mu)$ should go to unity when $U=0$, the correction can, for example, be encoded into the formula $z(\mu)=z_{SBMF}(\mu)[0.7+0.3z_{SBMF}(\mu)]$.

We finally would like to remark that the scheme defined by the set of linear equations for the coefficients (14)–(19) is absolutely robust as solutions exist for all regimes of parameters such as the strength of the interaction, doping, and degeneracy. In general, including any information on the self-energy $\Sigma(\omega_x)$ at some frequency point ω_x or its derivative $d\Sigma/d\omega|_{\omega=\omega_x}$ would generate a linear relationship between the interpolation coefficients, thus keeping the robustness of the method. On the other hand, fixing such relationships as the numbers of electrons brings nonlinearity to the problem, which could lead to multiplicity or nonexistence of solutions. It is also clear that by narrowing the regime of parameters, the accuracy of the interpolative algorithm can be systematically increased.

VI. CONCLUSION

To summarize, this paper shows the possibility of interpolating the self-energies for a whole range of dopings, degeneracies, and interactions using a computationally efficient algorithm. The parameters of the interpolation are obtained from a set of constraints in the slave-boson mean-field method combined with the functional form of the atomic Green's function. The interpolative method reproduces all trends in remarkable agreement with such a sophisticated and numerically accurate impurity solver as the QMC method. We also obtain a very good quantitative agreement in a whole range of parameters for such quantities as mean level occupancies, spectral functions, and self-energies. Some residual discrepancies remain, which can be corrected provided better algorithms delivering the constraints are utilized. Nevertheless, given the superior speed of the present approach, we have obtained a truly exceptional accuracy and efficiency of the proposed procedure.

ACKNOWLEDGMENTS

The work was supported by NSF-DMR Grants No. 0096462, No. 02382188, No. 0312478, and No. 0342290 and

by U.S. DOE Grant No. DE-FG02-99ER45761. The authors also acknowledge financial support from the Computational Material Science Network operated by U.S. DOE and from the Ministry of Education, Science and Sport of Slovenia.

APPENDIX

In the crystal-field case we assume that the N -fold degenerate impurity level ϵ_f is split by a crystal field into G sublevels $\epsilon_{f_1}, \dots, \epsilon_{f_\alpha}, \dots, \epsilon_{f_G}$. We assume that for each sublevel there is still some partial degeneracy d_α so that $\sum_{\alpha=1}^G d_\alpha = N$. In the limiting case of $SU(N)$ degeneracy, $G=1$, $d_1=N$, and in the nondegenerate case, $G=N$, $d_1=d_\alpha=d_G=1$. We need to discuss how a number of electrons n can be accommodated over different sublevels ϵ_{f_α} . Introducing the numbers of electrons in each sublevel, n_α , we obtain $\sum_{\alpha=1}^G n_\alpha = n$. Note the restrictions: $0 < n < N$, and $0 < n_\alpha \leq d_\alpha$. In the $SU(N)$ case, $G=1$, $n_1=n$, and in the nondegenerate case, $G=N$, and n_α is either 0 or 1. The total energy for the shell with n electrons depends on the particular configuration $\{n_\alpha\}$,

$$E_{n_1, \dots, n_G} = \sum_{\alpha=1}^G \epsilon_{f_\alpha} n_\alpha + \frac{1}{2} U(\sum_{\alpha} n_\alpha) [(\sum_{\alpha} n_\alpha) - 1]. \quad (\text{A1})$$

The many-body wave function is also characterized by a set of numbers $\{n_\alpha\}$, i.e., $|n_1, \dots, n_G\rangle$. The energy E_{n_1, \dots, n_G} remains degenerate, and can be calculated as the product of the number of combinations existing to accommodate the electrons in each sublevel, i.e., $C_{n_1}^{d_1} \times \dots \times C_{n_\alpha}^{d_\alpha} \times \dots \times C_{n_G}^{d_G}$. Let us further introduce the probability amplitudes ψ_{n_1, \dots, n_G} to find a shell in a given state with energy E_{n_1, \dots, n_G} . The sum of all probabilities should be equal to 1, i.e.,

$$\sum_{n_1=0}^{d_1} \dots \sum_{n_\alpha=0}^{d_\alpha} \dots \sum_{n_G=0}^{d_G} C_{n_1}^{d_1} \times \dots \times C_{n_\alpha}^{d_\alpha} \times \dots \times C_{n_G}^{d_G} \psi_{n_1, \dots, n_G}^2 = 1. \quad (\text{A2})$$

There are two Green's functions in the Gutzwiller method: the impurity Green's function $\hat{G}_f(i\omega)$ and the quasiparticle Green's function $\hat{G}_g(\omega) = \hat{b}^{-1} \hat{G}_f(\omega) \hat{b}^{-1}$, where the matrix coefficients \hat{b} represent generalized mass renormalization parameters. All matrices are assumed to be diagonal and have diagonal elements enumerated as follows: $G_1(\omega), \dots, G_\alpha(\omega), \dots, G_G(\omega)$. Each element in the Green's function is represented as follows:

$$G_{g\alpha}(\omega) = \frac{1}{\omega - \lambda_\alpha - b_\alpha^2 \Delta_\alpha(\omega)}, \quad (\text{A3})$$

$$G_{f\alpha}(\omega) = b_\alpha^2 G_{g\alpha}(\omega) \quad (\text{A4})$$

and determines the mean number of electrons in each sublevel,

$$\bar{n}_\alpha = d_\alpha T \sum_{i\omega} G_{g\alpha}(i\omega) e^{i\omega 0^+}. \quad (\text{A5})$$

The total mean number of electrons is thus $\bar{n} = \sum_{\alpha=1}^G \bar{n}_\alpha$. The hybridization function $\hat{\Delta}(i\omega)$ is a matrix that is assumed to be diagonal, and it has diagonal elements enumerated as follows: $\Delta_1(\omega), \dots, \Delta_\alpha(\omega), \dots, \Delta_G(\omega)$. The mass renormalizations $Z_\alpha = b_\alpha^2$ are determined in each sublevel.

The diagonal elements for the self-energy are

$$\begin{aligned} \Sigma_\alpha(\omega) &= \omega + \mu - \epsilon_{f_\alpha} - \Delta_\alpha(\omega) - G_\alpha^{-1}(\omega) \\ &= \omega \left(1 - \frac{1}{b_\alpha^2} \right) - \epsilon_{f_\alpha} - \frac{\lambda_\alpha}{b_\alpha^2}. \end{aligned} \quad (\text{A6})$$

Here,

$$\begin{aligned} b_\alpha &= R_\alpha L_\alpha \sum_{n_1=0}^{d_1} \dots \sum_{n_\alpha=1}^{d_\alpha} \dots \sum_{n_G=0}^{d_G} C_{n_1}^{d_1} \times \dots \times C_{n_\alpha}^{d_\alpha-1} \times \dots \\ &\quad \times C_{n_G}^{d_G} \psi_{n_1, \dots, n_\alpha, \dots, n_G} \psi_{n_1, \dots, n_\alpha-1, \dots, n_G}, \end{aligned} \quad (\text{A7})$$

$$\begin{aligned} L_\alpha &= \left(1 - \sum_{n_1=0}^{d_1} \dots \sum_{n_\alpha=1}^{d_\alpha} \dots \sum_{n_G=0}^{d_G} C_{n_1}^{d_1} \times \dots \times C_{n_\alpha}^{d_\alpha-1} \times \dots \right. \\ &\quad \left. \times C_{n_G}^{d_G} \psi_{n_1, \dots, n_\alpha, \dots, n_G}^2 \right)^{-1/2}, \end{aligned} \quad (\text{A8})$$

$$\begin{aligned} R_\alpha &= \left(1 - \sum_{n_1=0}^{d_1} \dots \sum_{n_\alpha=0}^{d_\alpha-1} \dots \sum_{n_G=0}^{d_G} C_{n_1}^{d_1} \times \dots \times C_{n_\alpha}^{d_\alpha-1} \times \dots \right. \\ &\quad \left. \times C_{n_G}^{d_G} \psi_{n_1, \dots, n_\alpha, \dots, n_G}^2 \right)^{-1/2}. \end{aligned} \quad (\text{A9})$$

The generalization of the nonlinear equations (23) has the form

$$\begin{aligned} 0 &= [E_{n_1, \dots, n_G} + \Lambda - (\sum_{\alpha}^G \lambda_\alpha n_\alpha)] \psi_{n_1, \dots, n_G} + \sum_{\alpha=1}^G n_\alpha [T \sum_{i\omega} \Delta_\alpha(i\omega) \\ &\quad \times G_{g\alpha}(i\omega)] b_\alpha [R_\alpha L_\alpha \psi_{n_1, \dots, n_\alpha-1, \dots, n_G} + b_\alpha L_\alpha^2 \psi_{n_1, \dots, n_\alpha, \dots, n_G}] \\ &\quad + \sum_{\alpha=1}^G (d_\alpha - n_\alpha) [T \sum_{i\omega} \Delta_\alpha(i\omega) G_{g\alpha}(i\omega)] \\ &\quad \times b_\alpha [R_\alpha L_\alpha \psi_{n_1, \dots, n_\alpha+1, \dots, n_G} + b_\alpha R_\alpha^2 \psi_{n_1, \dots, n_\alpha, \dots, n_G}]. \end{aligned} \quad (\text{A10})$$

- ¹For a review, see A. Georges, G. Kotliar, W. Krauth, and M. Rozenberg, *Rev. Mod. Phys.* **68**, 13 (1996).
- ²For a review, see, e.g., *Theory of the Inhomogeneous Electron Gas*, edited by S. Lundqvist and S. H. March (Plenum, New York, 1983).
- ³V. I. Anisimov, A. I. Poteryaev, M. A. Korotin, A. O. Anokhin, and G. Kotliar, *J. Phys.: Condens. Matter* **35**, 7359 (1997).
- ⁴A. Lichtenstein and M. Katsnelson, *Phys. Rev. B* **57**, 6884 (1998).
- ⁵G. Kotliar and S. Y. Savrasov, in *New Theoretical Approaches to Strongly Correlated Systems*, edited by A. M. Tsvelik (Kluwer Academic Publishers, Dordrecht, 2001), p. 259; S. Biermann, F. Aryasetiawan, and A. Georges, *Phys. Rev. Lett.* **90**, 086402 (2003).
- ⁶S. Y. Savrasov and G. Kotliar, *Phys. Rev. B* **69**, 245101 (2004).
- ⁷I. A. Nekrasov, K. Held, N. Blumer, A. I. Poteryaev, V. I. Anisimov, and D. Vollhardt, *Eur. Phys. J. B* **18**, 55 (2000).
- ⁸K. Held, G. Keller, V. Eyert, D. Vollhardt, and V. I. Anisimov, *Phys. Rev. Lett.* **86**, 5345 (2001).
- ⁹A. I. Lichtenstein, M. I. Katsnelson, and G. Kotliar, *Phys. Rev. Lett.* **87**, 067205 (2001).
- ¹⁰K. Held, A. K. McMahan, and R. T. Scalettar, *Phys. Rev. Lett.* **87**, 276404 (2001).
- ¹¹S. Savrasov, G. Kotliar, and E. Abrahams, *Nature (London)* **410**, 793 (2001).
- ¹²Xi Dai, S. Savrasov, G. Kotliar, A. Migliori, H. Ledbetter, and E. Abrahams, *Science* **300**, 953 (2003).
- ¹³S. Y. Savrasov and G. Kotliar, *Phys. Rev. Lett.* **90**, 056401 (2003).
- ¹⁴K. Held, I. A. Nekrasov, G. Keller, V. Eyert, N. Blumer, A. K. McMahan, R. T. Scalettar, Th. Pruschke, V. I. Anisimov, and D. Vollhardt, *Psi-k Newsletter* **56**, 65 (2003); A. I. Lichtenstein, M. I. Katsnelson, and G. Kotliar, in *Electron Correlations and Materials Properties*, edited by A. Gonis, N. Kioussis, and M. Ciftan (Kluwer Academic/Plenum Publishers, Dordrecht, 2002), p. 428.
- ¹⁵P. W. Anderson, *Phys. Rev.* **124**, 41 (1961).
- ¹⁶For a review, see, e.g., M. Jarrell and J. E. Gubernatis, *Phys. Rep.* **269**, 133 (1996).
- ¹⁷H. Jeschke and G. Kotliar, cond-mat/0406472 (unpublished).
- ¹⁸S. Florens and A. Georges, *Phys. Rev. B* **66**, 165111 (2002).
- ¹⁹K. Haule, S. Kirchner, J. Kroha, and P. Wölfle, *Phys. Rev. B* **64**, 155111 (2001).
- ²⁰S. H. Vosko, L. Wilk, and M. Nusair, *Can. J. Phys.* **58**, 1200 (1980).
- ²¹D. M. Ceperley and B. J. Alder, *Phys. Rev. Lett.* **45**, 566 (1980).
- ²²M. Gutzwiller, *Phys. Rev.* **134**, A923 (1964).
- ²³G. Kotliar and A. E. Ruckenstein, *Phys. Rev. Lett.* **57**, 1362 (1986).
- ²⁴R. Fresard and G. Kotliar, *Phys. Rev. B* **56**, 12909 (1997).
- ²⁵H. Hasegawa, *Phys. Rev. B* **56**, 1196 (1997).
- ²⁶J. Hubbard, *Proc. R. Soc. London, Ser. A* **281**, 401 (1964).
- ²⁷R. Bulla, T. A. Costi, and D. Vollhardt, *Phys. Rev. B* **64**, 045103 (2001).
- ²⁸S. Florens, A. Georges, G. Kotliar, and O. Parcollet, *Phys. Rev. B* **66**, 205102 (2002).
- ²⁹See, e.g., D. D. Johnson, *Phys. Rev. B* **38**, 12807 (1988).
- ³⁰W. Nolting and W. Borgiel, *Phys. Rev. B* **39**, 6962 (1989).
- ³¹L. M. Roth, *Phys. Rev.* **184**, 451 (1969).